



Trans. Nonferrous Met. Soc. China 32(2022) 1795-1804

Transactions of Nonferrous Metals Society of China

www.tnmsc.cn



E2EM's prediction of LaB₆ as nucleation substrate for primary Mn-rich phase in Al–Si–Cu–Mn heat-resistant alloy and its refining effect

Guang-jing LI, Heng-cheng LIAO

Jiangsu Key Laboratory of Advanced Metallic Materials, School of Materials Science and Engineering, Southeast University, Nanjing 211189, China

Received 22 June 2021; accepted 15 October 2021

Abstract: Edge-to-edge matching (E2EM) model was used to predict the potency of LaB₆ as the heterogeneous nucleation substrate for primary Al₁₃Mn₄Si₈ phase formed during the solidification of Al–Si–Cu–Mn heat-resistant alloy. There are five pairs of orientation relationships (ORs) between LaB₆ and Al₁₃Mn₄Si₈ phases which meet the criteria of E2EM model. One pair of plane ORs ((110)_{LaB₆}//(110)_{Al₁₃Mn₄Si₈) are demonstrated by TEM observation. This strongly indicates that the LaB₆ phase can act as the heterogeneous nucleation substrate for the primary Al₁₃Mn₄Si₈ phase. 1.0 wt.% of Al–2La–1B master alloy was also added into Al–12Si–4Cu–2Mn alloy to evaluate the refining effect by microstructure observation and tensile test. Experimental results show that addition of Al–2La–1B master alloy can significantly refine the primary Al₁₃Mn₄Si₈ phase, supporting the prediction accuracy of E2EM model. However, such refinement of primary Al₁₃Mn₄Si₈ phase does not lead to an improvement in strength. This is due to the larger difference in elastic modulus between the finally formed Al₁₃Mn₄Si₈ phase and aluminum matrix than that of Al₁₅Mn₃Si₂ phase. **Key words:** edge-to-edge model; Al₁₃Mn₄Si₈ phase; LaB₆ phase; heat-resistant aluminum alloy; microstructure; mechanical property}

1 Introduction

In recent years, heat-resistant aluminum alloys are developing rapidly along with the development of automobile and space industries. At present, Al-Si-Cu-Mg heat-resistant alloys have been widely used to manufacture engines for small passenger cars, for examples, A380, 319 and ZL702A [1-4]. In these alloys, CuAl₂ phase acts as the main heat-resistant strengthening phase, along with $Al_4CuMg_5Si_4$ (*W*-phase), Al₅Mg₈Si₆Cu₂ (Q-phase) and some other complex intermetallic compound phases formed during the solidification and various heat treatment processes. To further improve the heat resistance of those aluminum alloys, new heat-resistant phases have been designed. For example, it has been reported that adding Fe and Ni (and therefore introducing Fe-rich phase and Ni-rich phase respectively) can effectively increase the thermal resistance [5,6].

LIAO et al [7] developed a novel heat-resistant alloy by adding excessive amount of Mn in a near eutectic Al-12Si-4Cu alloy to form primary Mn-rich phase. SUO et al [8] reported that this Mn-rich phase has excellent thermal stability up to 20 h at 798 K, which strongly indicates that it can act as the heat-resistant strengthening phase. LI et al [9] found that there are two types of primary Mn-rich phases in Al-12Si-4Cu-2Mn system: the lath-like Al₁₃Mn₄Si₈ phase and dendritic Al₁₅Mn₃Si₂ phase. The dendritic Al₁₅Mn₃Si₂ phase is formed from the lath-like Al₁₃Mn₄Si₈ phase by a peritectic reaction: L+Al₁₃Mn₄Si₈ phase by a peritectic reaction: L+Al₁₃Mn₄Si₈ phase of Mn on the tensile property of Al-12Si-4Cu-xMn alloys at

both ambient and elevated temperatures, with strengths of 263 and 125 MPa at room temperature and 573 K respectively when Mn content reached 1.2 wt.%. However, further increase in Mn content would result in a decrease in strength, duo to the appearance of coarse primary Mn-rich dendritic structure. Thus, to further improve the high temperature strength of Al–Si–Cu–Mn system alloys, refining the primary Mn-rich phase has both academic and industrial interest.

Al-La-B master alloy has been paid more attention as a new refiner recently. This master alloy combines excellent refining effects of B and La in Al-Si casting alloys, yet eliminates the multi-poisoning effect between B and Sr [13-15]. LI et al [16] prepared an Al-3wt.%LaB₆ master alloy by a melting reaction method and studied its refining effect in A390 alloy. They also employed edge-to-edge matching (E2EM model) to evaluate the orientation relationship (OR) between LaB₆ and α-Al phases and concluded that Al-3wt.%LaB₆ master alloy could effectively refine the primary α -Al phase in industrially pure aluminum [17]. Similarly, JING et al [18,19] prepared a new Al-2La-1B master alloy refiner and reported a considerable refinement of primary α -Al dendrites in Al-10Si-0.3Mg and Al-7Si-0.3Mg alloys by 1.0 wt.% of Al-2La-1B master alloy.

The E2EM model was initially proposed and further developed by ZHANG et al [20–23]. This model predicts the matching effect between two phases through quantitatively comparing the lattice structure, lattice constant, and atomic position, and subsequently evaluates the potency of the heterogeneous nucleation substrates. This model successfully explains the mechanisms of various grain refinement behaviors and has been used to predict the crystallographic characteristics of the diffusion-controlled phase transformation. The details about E2EM model are seen in Ref. [20].

Since E2EM model was proposed, it has been widely used to predict the potency of refiners in aluminum and magnesium alloys. ZHANG et al [20] calculated the mismatching degree of Al₃Ti, TiC, TiB₂ and AlB₂ crystals with α-Al crystal through E2EM model and concluded that Al₃Ti has stronger refining ability than TiC, TiB₂ and AlB₂. The results are in good agreement with experimental observations. By E2EM model, Al₄C₃, Al₂CO and Al₈(Mn,Fe)₅ phases have also been illustrated to

have a potency to refine Mg-Al alloys [23]. Among them, the potency of Al₂CO phase is the largest and Al₈(Mn, Fe)₅ phase is the lowest. E2EM model has also been used to predict the habit plane precipitation behaviors [21,22]. QIU et al [24] used E2EM model to conclude that Al₂Y phase has good orientation relationships with α -Mg phase in Mg alloys, which was verified by adding a certain amount of Al to the Mg-Y alloy. Using E2EM model, QIU et al [25] explained the poisoning mechanism of Zr element to Ti-refiner in aluminum alloys. XIAO et al [26] revealed the poisoning mechanism of Zr element on Al-Ti-C and Al-Ti-B master alloys. WANG et al [27,28] reported that Al₃Nb and Al₃Zr phases have good orientation relationships with α -Al phase. The Δg parallelism criteria is another method to predict the potential preferred orientation relationships of nucleus/ substrate during the nucleation and growth of crystal [29]. This is more elaborate than the E2EM model and can be used to refine the possible ORs. However, it is more complex too.

As described above, E2EM model is usually used to predict the heterogeneous nucleation potency of the potential refiners for primary metallic phases (primary Al and Mg phases in Al alloys and Mg alloys, respectively). However, there are few studies on using E2EM model to seek the efficient refiners for primary intermetallic compound phases. Thus, it is very meaningful to applying E2EM model to the study of intermetallic compounds refinement. Besides, the effect of the refinement of intermetallic compounds on the heat resistance of heat-resistant alloys is unclear. In Al-12Si-4Cu-2Mn alloy, the first primary phase is Al₁₃Mn₄Si₈ phase, a coarse needle-like intermetallic compound with a simple tetragonal structure of a=b=1.240 nm and c=0.489 nm [10]. LaB₆ phase in Al-La-B master alloy is always thought to act as the heterogeneous nucleation substrates for primary α-Al phase. People do not know whether LaB₆ can be used to refine Al₁₃Mn₄Si₈ phase or not. Thus, it is very meaningful to applying E2EM model to evaluating the potency of LaB6 phases as the nucleation substrate for Al₁₃Mn₄Si₈ phase. The effect of the refinement of Al₁₃Mn₄Si₈ phase on the high temperature strength of Al-Si-Cu-Mn alloy is also interesting. So, in this study, the ORs between LaB₆ and Al₁₃Mn₄Si₈ phase were evaluated by E2EM model, and Al-La-B master alloy was added into Al-12Si-4Cu-2Mn alloy to verify its refining effect, and the tensile test at different temperatures was implemented to study the refinement of intermetallic compounds on the high-temperature strength of heat-resistant alloy.

2 Experimental

2.1 Alloy preparation

In this work, SCO (without addition of Al-2La-1B refiner) and SC0-L (with addition of the refiner) alloys were prepared by using Al-20wt.%Si, Al-20wt.%Cu and Al-10wt.%Mn master alloys and pure aluminum ingot as raw materials. After processing, 1.0 wt.% of Al-2La-1B master alloy was added into the melt at about 993 K, and then the melt was poured into an iron mold (with a plate-like cavity of 170 mm × $100 \text{ mm} \times 20 \text{ mm}$, preheated at 523 K for 5 h). Al-2La-1B master alloy was fabricated as Ref. [18], using Al-10wt.%La and Al-3wt.%B master alloy as the raw materials. The chemical composition of the studied alloys was measured by MAXx LMF15 spark emission spectrometer, [30], Al-12.01wt.%Si-3.53wt.%Cu-2.12wt.%Mn; SC0-L, Al-12.30wt.%Si-3.79wt.%Cu-2.09wt.% Mn-0.014wt.%La-0.019wt.%B.

2.2 Microstructure observation and tensile test

Metallographic samples were cut from the castings and were etched with a mix acid reagent (20 vol.% HCl + 20 vol.% HNO₃ + 5 vol.% HF + 55 vol.% H₂O) for 15 s. Microstructure observation was carried out using OLYMPUS BX60M metallographic microscope, scanning electron microscopy (SEM, Sirion) equipped with EDS and elements-mapping with 20.0 kV observed voltage, and transmission electron microscope (TEM, G²20) equipped with EDS and SAED with 200.0 kV observed voltage. The sample for TEM observation

was fabricated by focused ion beam (FIB, Helios nanolab 600, FEI) technique. The plate specimens for tensile test were also cut from the casting, with a gauge size of 18 mm × 3 mm × 3 mm. All tensile specimens were undergone with the same heat treatment of solutionizing at 783 K for 5 h + aging at 483 K for 6 h [7]. The tensile test was carried out on a CMT5105 tester with a rate of 1 mm/min at room temperature, 423, 523, 573 and 623 K (before testing, the samples were held at these temperatures for 30 min), and the ultimate tensile strength is taken as an average of three parallel samples.

3 Results and discussion

3.1 Orientation relationships between LaB₆ and Al₁₃Mn₄Si₈ phases predicted by E2EM model

Al₁₃Mn₄Si₈ phase is the first formed primary Mn-rich phase in Al-12Si-4Cu-2Mn alloy, and its crystal structure is determined to be a simple tetragonal with lattice constants of a=b=1.243 nm, c=0.489 nm, and $\alpha=\beta=\gamma=90^{\circ}$ [10], in which, the atoms locate the eight apexes of the hexahedron. The atom close-packed or nearly close-packed directions of this phase are (001), (100), (101) and $\langle 110 \rangle$. The crystal structure of LaB₆ is a simple cube with a lattice constant of a=0.416 nm [18]. La atoms in LaB6 occupy eight apexes of the hexahedron and B atoms locate the interstices. But compared with La, the atomic radius of B is very small, so when considering the close-packing direction, only ones of La atoms are taken into account [17]. The unit cell of LaB6 phase is much smaller than that of Al₁₃Mn₄Si₈ phase. For the convenience to find the potential matching relationships, the unit cell of LaB₆ phase is enlarged in the form of 3×3×1 cells, as shown in Fig. 1.

Both the LaB₆ and Al₁₃Mn₄Si₈ phases are intermetallic compound with constant composition,

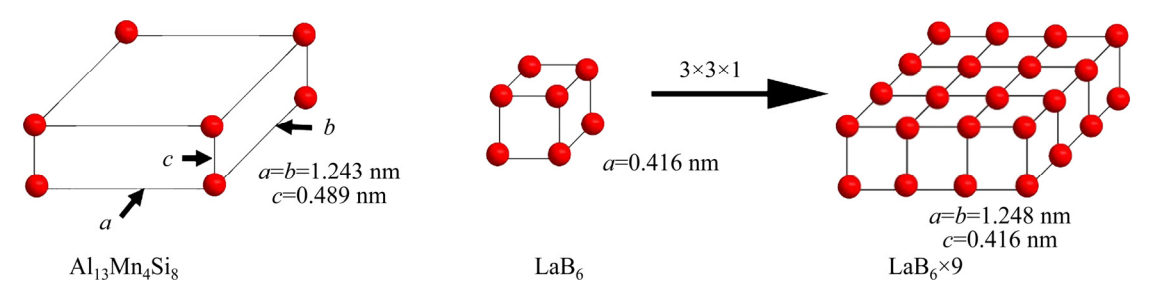


Fig. 1 Schematics of crystal structures of Al₁₃Mn₄Si₈ and LaB₆ phases

so the interatomic spacing of them is usually thought to be constant. According to the lattice constants of Al₁₃Mn₄Si₈ and LaB₆ phases, the values of the interatomic spacing in the close-packed or nearly close-packed directions of two cells (see Fig. 1) are calculated, as listed in Table 1.

Thus, the atom row mismatch degrees $(f_{\rm d})$ of the close-packed or nearly close-packed directions between Al₁₃Mn₄Si₈ and LaB₆ phases, are calculated, as summarized in Table 2. $f_{\rm d} = (d_{\rm A} - d_{\rm B})/d_{\rm A} \,|\,$ [20], where d is the interatomic spacing of the close-packed or near close-packed directions, and subscript A and B

Table 1 Close-packed or nearly close-packed directions of two cells shown in Fig. 1 and interatomic spacing of them

Direction	$d_{\rm A}/{ m nm}$	$d_{\rm L3}/{\rm nm}$
⟨001⟩	0.489	0.416
$\langle 100 \rangle$	1.243	1.248
⟨101⟩	1.336	1.316
⟨110⟩	1.758	1.764

Note: The subscript A of d_A represents the unit cell of Al₁₃Mn₄Si₈ phase, and the subscript L3 of d_{L3} represents the enlarged LaB₆ cell in $3\times3\times1$ mode as shown in Fig. 1

Table 2 Atom row mismatch degrees of close-packed or nearly close-packed directions between Al₁₃Mn₄Si₈ and LaB₆ phases

Direction	$f_{ m d}$ /%			
	$\langle 001\rangle_A$	$\langle 100 \rangle_{\!A}$	$\langle 101 \rangle_A$	$\langle 110 \rangle_A$
$\langle 001\rangle_{L3}$	14.93	66.53	68.86	76.34
$\langle 100 \rangle_{L3}$	155.21	0.32	6.59	29.01
$\langle 101\rangle_{L3}$	169.12	5.87	1.50	25.14
$\langle 110 \rangle_{L3}$	260.74	41.91	32.04	0.34

mark the A and B phases respectively. There are five groups of atom row pairs that meet the minimum matching requirement of E2EM model $(f_d < 10\%)$, namely, $\langle 100 \rangle_A / \langle 100 \rangle_{L3}$, $\langle 100 \rangle_A / \langle 101 \rangle_{L3}$, $\langle 101 \rangle_A / \langle 101 \rangle_{L3}$ and $\langle 110 \rangle_A / \langle 110 \rangle_{L3}$.

The close-packed or nearly close-packed planes of a simple tetragonal are (001), (110) and (010). The atom row close-packed or nearly close-packed directions, (001), (100), (101) and (110), are all in them, as shown in Fig. 2. The inter-planar spacings of close-packed or nearly close-packed planes of Al₁₃Mn₄Si₈ and LaB₆ phases are tabulated in Table 3. Based on it, the plane mismatch degrees, f_p , are calculated, as summarized in Table 4. $f_p = |(p_A - p_B)/p_A|$ [20], where p is the inter-planar spacing of the close-packed near close-packed planes and subscript A and B mark the A and B phases respectively. It is seen that there are groups of atom close-packed or nearly close-packed planes between Al₁₃Mn₄Si₈ and LaB₆ phases that meet the matching requirement of E2EM model ($f_p < 6\%$), i.e. $(110)_A / (110)_{L3}$ and $(010)_A$ // $(010)_{L3}$. For the atom row close-packed or nearly close-packed directions, $\langle 001 \rangle$ and $\langle 110 \rangle$ are contained in the crystal plane of (110), and (001), $\langle 100 \rangle$ and $\langle 101 \rangle$ are contained in the crystal plane of (010).

Based on the E2EM model, there are five groups of ORs between Al₁₃Mn₄Si₈ and LaB₆ phases that meet the criteria, as

$$\begin{split} &(110)_{A} /\!/(110)_{L3} \!: \langle 110\rangle_{A} /\!/\langle 110\rangle_{L3}; \\ &(010)_{A} /\!/(010)_{L3} \!: \langle 100\rangle_{A} /\!/\langle 100\rangle_{L3}, \langle 100\rangle_{A} /\!/\langle 101\rangle_{L3}, \\ &\qquad \qquad \langle 101\rangle_{A} /\!/\langle 100\rangle_{L3}, \langle 101\rangle_{A} /\!/\langle 101\rangle_{L3} \end{split}$$

The above results indicate that there is a good matching relationship between the Al₁₃Mn₄Si₈ and LaB₆ phases. That is, the LaB₆ particles in

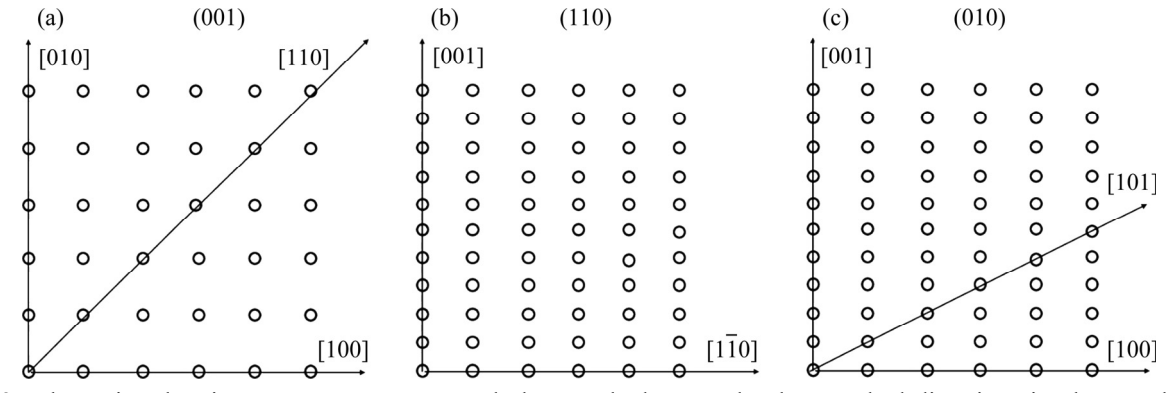


Fig. 2 Schematics showing atom arrangement and close-packed or nearly close-packed directions in close-packed or nearly close-packed planes of simple tetragonal structure: (a) (001); (b) (110); (c) (010)

Table 3 Inter-planar spacing of close-packed or nearly close-packed planes of Al₁₃Mn₄Si₈ and LaB₆ phases

Plane	$p_{ m A}/{ m nm}$	$p_{ m L3}$ /nm
(001)	0.489	0.416
(110)	0.879	0.882
(010)	1.243	1.248

Table 4 Plane mismatch degree of close-packed or nearly close-packed planes between $Al_{13}Mn_4Si_8$ and LaB_6 phases

Plane	$f_{ m p}/\%$ o			
	$(001)_{A}$	$(110)_{A}$	$(010)_{A}$	
$(001)_{L3}$	14.93	52.67	66.53	
$(110)_{L3}$	80.37	0.34	29.04	
$(010)_{L3}$	155.21	41.98	0.32	

Al-2La-1B master alloy are expected to have a strong ability as the heterogeneous nucleation substrates for the primary $Al_{13}Mn_4Si_8$ phase in Al-12Si-4Cu-2Mn heat-resistant alloy.

3.2 Refinement effect of Al-2La-1B master alloy on primary Al₁₃Mn₄Si₈ phase

The optical microscopy images in Fig. 3 reveal that addition of 1.0 wt.% Al–2La–1B master alloy has a significant influence on the morphology and size of the primary Mn-rich phases. In SC0 alloy without addition of Al–2La–1B master alloy (as a refiner), primary Mn-rich phases have two morphologies, a large number of dendrites and a small number of slender rods (Fig. 3(a)), and its SEM images and EDS results are shown in Figs. 4(a–c). For the dendrites, the Si/Mn mole ratio is close to Al₁₅Mn₃Si₂ phase reported in Refs. [7,8,10,29], and for the slender rods, it is similar and close to Al₁₃Mn₄Si₈ [9,10]. The dendritic

ones are Al₁₅Mn₃Si₂ phase and the slender rod-like ones are Al₁₃Mn₄Si₈ phase. The length of slender $Al_{13}Mn_4Si_8$ rods is in the range of 100–300 µm (in a rough estimation) with a width range of $5-15 \mu m$. In SC0-L alloy with the addition of 1.0 wt.% Al-2La-1B refiner, the primary Mn-rich phase is completely different. Only a great amount of fine short-rod-like particles (Figs. 3(b) and Fig. 4(d)) are observed. The EDS result of those fine particles (see Figs. 4(e)) illustrates almost the same composition as the slender rods (Fig. 4(c)). In SC0-L alloy, only one primary Mn-rich phase is formed, that is Al₁₃Mn₄Si₈. The length of it is significantly shortened, in a range of 15-50 µm with a width range of 5–30 μm. So, the addition of Al-2La-1B refiner in Al-12Si-4Cu-2Mn alloy leads to two impacts: a complete suppression on the formation of Al₁₅Mn₃Si₂ phase, and a significant refinement on the Al₁₃Mn₄Si₈ phase.

Luckily, a bright particle about 3 µm is found to locate within a short-rod-like Al₁₃Mn₄Si₈ particle (Fig. 5(a)). EDS results (Figs. 5(b, c)) and element mapping images (Fig. 5(d)) illustrate that the short-rod particle is the primary Al₁₃Mn₄Si₈ phase and the bright particle contains very high La and B which means LaB₆ particle. This verifies that LaB₆ particle can act as the heterogeneous nucleation substrate for Al₁₃Mn₄Si₈ phase. According to the E2EM model, the good matching relationship between Al₁₃Mn₄Si₈ and LaB₆ phases reveals that LaB₆ phase has a great potency to act as the heterogeneous nucleation substrate for Al₁₃Mn₄Si₈ phase. Therefore, when the Al-2La-1B refiner was added into the Al-12Si-4Cu-2Mn alloy melt, a large amount of fine LaB₆ particles were released. Because Al₁₃Mn₄Si₈ phase is the first formed primary phase during the solidification of Al-12Si-4Cu-2Mn alloy [10], it first nucleates and grows on

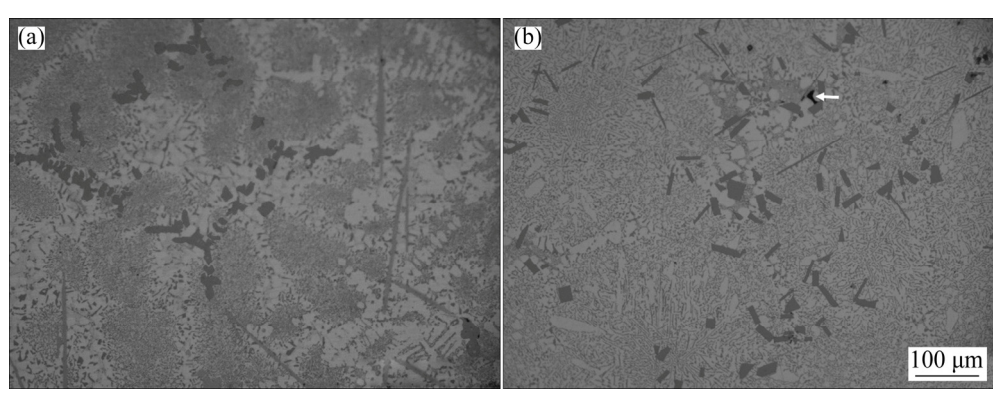


Fig. 3 Optical microscopy images of as-cast SC0 (a) and SC0-L (b) alloys

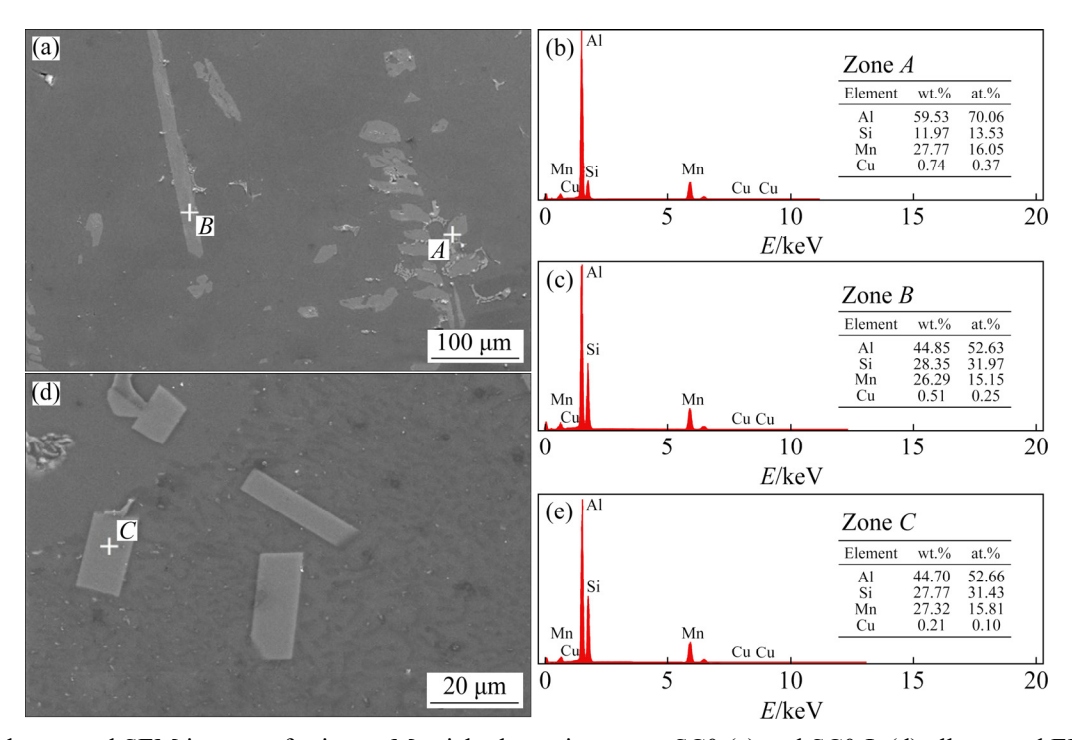


Fig. 4 Backscattered SEM images of primary Mn-rich phases in as-cast SC0 (a) and SC0-L (d) alloys, and EDS results of Zone A (b), Zone B (c) and Zone C (e)

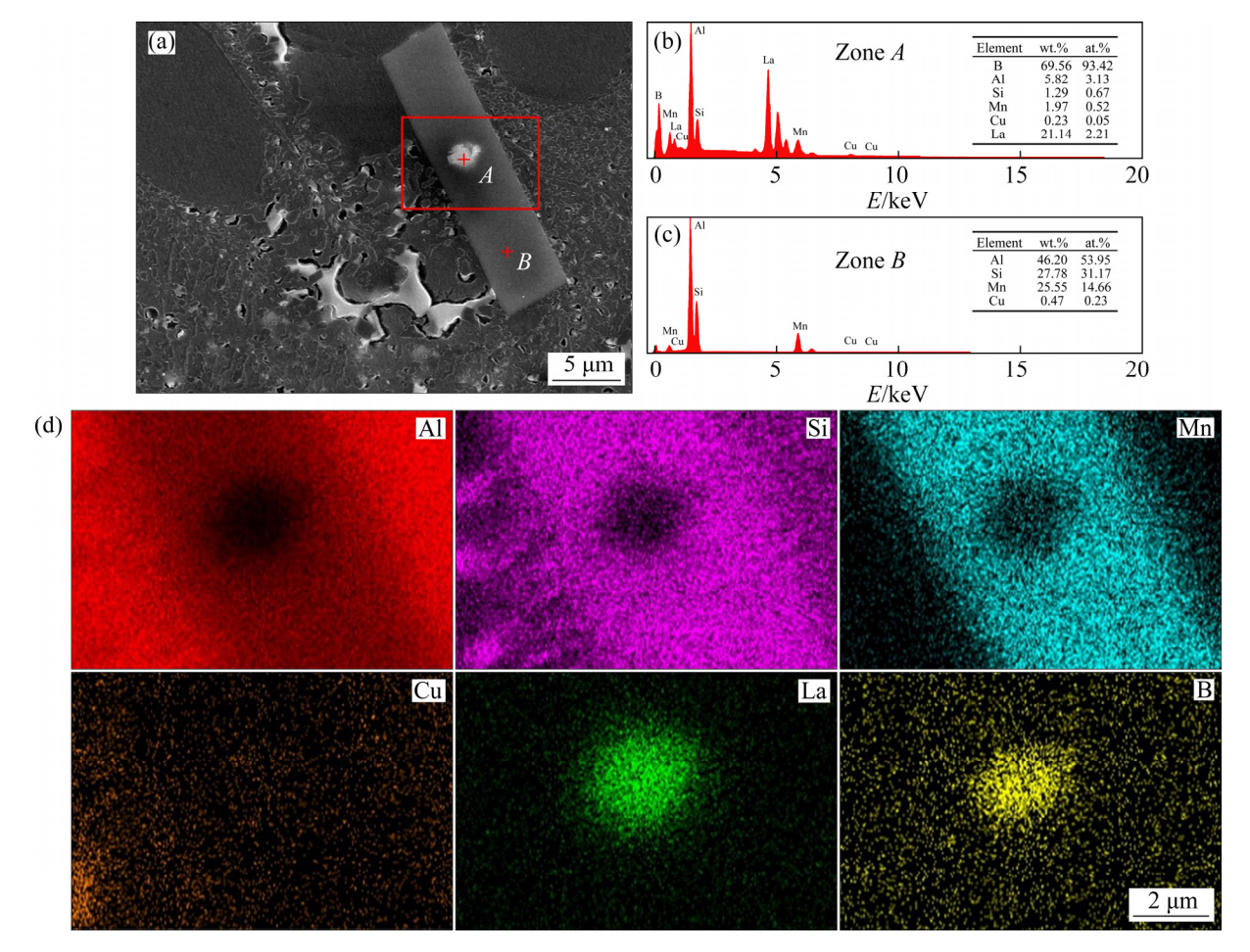


Fig. 5 Backscattered SEM image showing short-rod particle of primary Mn-rich phase and inserted LaB₆ particle in SC0-L alloy (a), EDS results of Zones A and B (b, c), and elements mapping images corresponding to red wireframe (d)

the surface of LaB₆ particle. Due to a great amount of Al₁₃Mn₄Si₈ crystals nucleate simultaneously, the growing space of them is limited extremely, thus they grow as short-rod-like (Fig. 3(b)), instead of slender-rod-like (see Fig. 3(a)). As a result, the primary Al₁₃Mn₄Si₈ phase was significantly refined. For the SC0 alloy, during the solidification, the first formed Al₁₃Mn₄Si₈ phase would transform into Al₁₅Mn₃Si₂ phase by a peritectic reaction: $L+Al_{13}Mn_4Si_8 \rightarrow Al_{15}Mn_3Si_2$ [10]. But, for the SC0-L alloy, this peritectic reaction is completely suppressed. The reason for it may be due to the slight change in structure of new formed Al₁₃Mn₄Si₈ phase on LaB₆ particle, or, more likely, due to the variation of liquid properties induced by trace La or B solutes in liquid. These factors make Al₁₅Mn₃Si₂ phase hard to nucleate on Al₁₃Mn₄Si₈ particles. The physic mechanism is not clear now which needs further study.

To further study the refinement mechanism and confirm the result of E2EM model, the film

sample containing a structure of Al-matrix and Al₁₃Mn₄Si₈ and LaB₆ phases was fabricated by FIB technique and observed through TEM. The bright image in Fig. 6(a) shows that LaB₆ phase contacts with Al₁₃Mn₄Si₈ phase in Al-matrix (confirmed by SAED patterns shown in Figs. 6(b) and (c), respectively). Although the ideal orientation relationships between the Al₁₃Mn₄Si₈ phase and LaB₆ phase cannot be illustrated directly from this sample due to the observation angle limitation of the G²20 machine, luckily, the (110) planes in both LaB₆ phase (Fig. 6(b)) and Al₁₃Mn₄Si₈ phase (see Fig. 6(c)) from their $[1\overline{12}]$ zone axis are observed. The relationship between (110)_{LaB_e} and $(110)_{Al_{13}Mn_4Si_8}$ can be confirmed through rotating the angle of the SAED image of LaB6 phase (clockwise rotation 79.8°). As shown in Fig. 6(d), one relationship between orientation LaB_6 $Al_{13}Mn_4Si_8$ phases is found as $(110)_{LaB_6}$ // (110)_{Al₁₃Mn₄Si₈}, which is one of two groups of plane ORs between Al₁₃Mn₄Si₈ and LaB₆ phases predicted

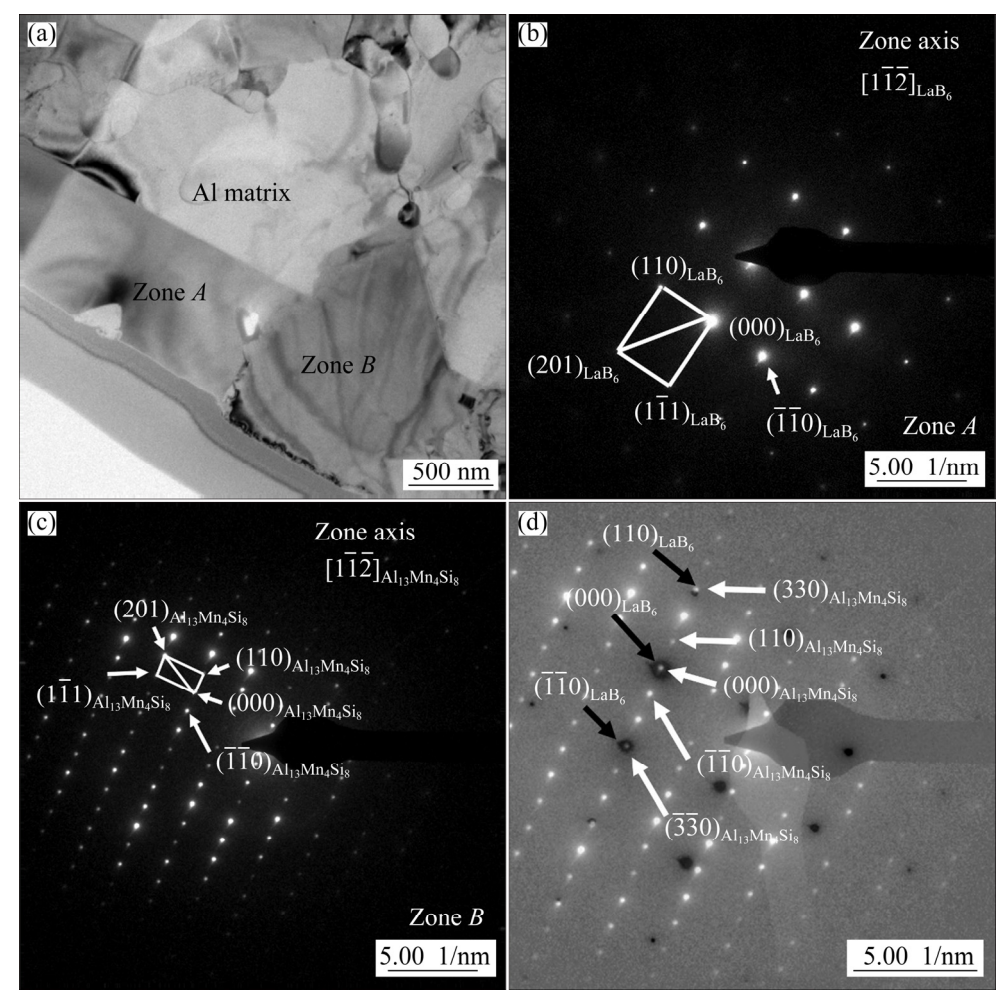


Fig. 6 Bright field TEM image showing $Al_{13}Mn_4Si_8$ and LaB_6 phases in Al matrix of SC0-L alloy (a), and SAED results corresponding to Zones A (b) and B (c) and superimposed image obtained by rotation (d)

by E2EM model. According to the lattice constants of LaB₆ and Al₁₃Mn₄Si₈ phases, $d(110)_{\text{LaB}_6} = d(\overline{1}\,\overline{1}0)_{\text{LaB}_6} = 0.294$ nm, $d(110)_{\text{Al}_{13}\text{Mn}_4\text{Si}_8} = d(\overline{1}\,\overline{1}0)_{\text{Al}_{13}\text{Mn}_4\text{Si}_8} = 0.879$ nm, and $d(330)_{\text{Al}_{13}\text{Mn}_4\text{Si}_8} = d(\overline{3}\,\overline{3}0)_{\text{Al}_{13}\text{Mn}_4\text{Si}_8} = 0.293$ nm. It is known that the plane spacing is inversely proportional to the distance between the diffraction spots in SAED, thus, the diffraction spots of $(110)_{\text{LaB}_6}$ and $(\overline{1}\,\overline{1}0)_{\text{LaB}_6}$ should overlap the $(330)_{\text{Al}_{13}\text{Mn}_4\text{Si}_8}$ and $(\overline{3}\,\overline{3}0)_{\text{Al}_{13}\text{Mn}_4\text{Si}_8}$, as show in Fig. 6(d).

Based on the prediction of E2EM model, there are five groups of ORs between Al₁₃Mn₄Si₈ and LaB₆ phases on (110) and (010) planes; however, only one OR on (110) is observed by TEM due to the sample angle limitation. Even so, this demonstrates the accuracy of E2EM model too.

3.3 Effect of refinement of primary Mn-rich phase on tensile strength

Tensile strengths of the SC0 and SC0-L alloys after T6 treatment are listed in Table 5. Although the addition of Al-2La-1B refiner produces a significant refining effect on the primary Mn-rich phases, from the coarse dendrites (Al₁₅Mn₃Si₂) and slender rods (Al₁₃Mn₄Si₈) into the fine short-rod particles (Al₁₃Mn₄Si₈), the strength of SC0-L alloy is almost equal to or a little less than that of the SC0 alloy at different temperatures of tensile test. That is, the significant refinement of the primary Mn-rich phases does not lead to an expected improvement in strength. However, the refinement of primary Mn-rich phase induced by Cr-alloying Al-12Si-4Cu-2Mn alloys leads considerable increase in strength, especially at high temperatures [30]. It is worth to note that, in the case of Cr-alloying induced refinement, the final formed primary Mn-rich phase is Al₁₅Mn₃Si₂, but not Al₁₃Mn₄Si₈ in SC0-L alloy. LI et al [9] evaluated the contribution of these two primary Mn-rich phases to strength, and thought that the contribution from Al₁₅Mn₃Si₂ phase is larger than Al₁₃Mn₄Si₈ phase whether at room temperature or at high temperatures. The reason for it is thought to be tied with the much larger difference in elastic modulus of Al₁₃Mn₄Si₈ phase with aluminum matrix than that of Al₁₅Mn₃Si₂ [9]. So, in this study, because the finally formed primary Mn-rich phase in SC0-L alloy is still Al₁₃Mn₄Si₈ phase, the strength of SC0-L alloy is not improved even though this Mn-rich phase is refined significantly.

On the other hand, it implies that to promote the peritectic transformation from Al₁₃Mn₄Si₈ to Al₁₅Mn₃Si₂ is very important at the same time of refining the primary Mn-rich phase.

Table 5 Ultimate tensile strength (UTS) of studied alloys at different temperatures of tensile test

		UTS	S/MPa		
Alloy	Room	123 K	523 K	573 K	623 K
	temperature	423 K	323 K	373 K	023 K
SC0 [30]	191±6.5	179±4.5	146±1.0	119±6.4	83±1.0
SC0-L	181 ± 8.9	175±0.3	158±7.0	118±0.1	81±4.6

4 Conclusions

- (1) There are five groups of ORs between Al₁₃Mn₄Si₈ and LaB₆ phases, which well meets the criteria of E2EM model, suggesting that LaB₆ phase has a strong potency to act as a heterogeneous nucleation substrate for the primary Al₁₃Mn₄Si₈ phase in Al-12Si-4Cu-2Mn heat-resistant alloy. TEM observation demonstrates one OR on (110) between Al₁₃Mn₄Si₈ and LaB₆ phases.
- (2) Adding 1.0 wt.% Al-2La-1B master alloy in Al-12Si-4Cu-2Mn alloy can significantly refine the primary Al₁₃Mn₄Si₈ phase, yet completely suppresses the peritectic reaction. This confirms the prediction by E2EM model.
- (3) The significant refinement on the primary Al₁₃Mn₄Si₈ phase in Al-12Si-4Cu-2Mn alloy does not lead to an improvement in strength. This is due to the larger difference in elastic modulus between Al₁₃Mn₄Si₈ phase and aluminum matrix than that of Al₁₅Mn₃Si₂ phase.

Acknowledgments

This work was supported by Jiangsu Key Laboratory Metallic Materials, China (No. BM2007204), and the Fundamental Research Funds for the Central Universities, China (No. 2242016k40011)

References

[1] ZHANG Jia-ying, ZUO Li-jie, FENG Jian, YE Bing, KONG Xiang-yang, JIANG Hai-yan, DING Wen-jiang. Effect of thermal exposure on microstructure and mechanical properties of Al-Si-Cu-Ni-Mg alloy produced by different casting technologies [J]. Transactions of Nonferrous Metals Society of China, 2020, 30: 1717–1730.

- [2] MAN Jin, JING Li, JIE Shao-guang. The effects of Cu addition on the microstructure and thermal stability of an Al-Mg-Si alloy [J]. Journal of Alloys and Compounds, 2007, 437(1/2): 146-150.
- [3] ABDULWAHAB M, MADUGU I A, YARO S A, HASSAN S B, POPOOLA A P I. Effects of multiple-step thermal ageing treatment on the hardness characteristics of A356. 0-type Al-Si-Mg alloy [J]. Materials & Design, 2011, 32(3): 1159-1166.
- [4] RINCON E, LOPEZ H F, CISNEROS M M, MANCHA H. Temperature effects on the tensile properties of cast and heat treated aluminum alloy A319 [J]. Materials Science and Engineering A, 2009, 519(1/2): 128–140.
- [5] ASGHAR Z, REQUENA G, KUBEL F. The role of Ni and Fe aluminides on the elevated temperature strength of an AlSi₁₂ alloy [J]. Materials Science and Engineering A, 2010, 527(21/22): 5691–5698.
- [6] LI Yun-guo, YANG Yang, WU Yu-ying, WANG Li-yan, LIU Xiang-fa. Quantitative comparison of three Ni-containing phases to the elevated-temperature properties of Al–Si piston alloys [J]. Materials Science and Engineering A, 2010, 527(26): 7132–7137.
- [7] LIAO Heng-cheng, TANG Yun-yi, SUO Xiao-jing, LI Guang-jin, HU Yi-yun, DISIT U S, PETROV P. Dispersoid particles precipitated during the solutionizing course of Al-12wt.%Si-4wt.%Cu-1.2wt.%Mn alloy and their influence on high temperature strength [J]. Materials Science and Engineering A, 2017, 699: 201–209.
- [8] SUO Xiao-jing, LIAO Heng-cheng, HU Yi-yun, DIXIT U S, PETROV P. Formation of Al₁₅Mn₃Si₂ phase during solidification of a novel Al-12%Si-4%Cu-1.2%Mn heatresistant alloy and its thermal stability [J]. Journal of Materials Engineering and Performance, 2018, 27(6): 2910-2920.
- [9] LI Guang-jing, LIAO Heng-cheng, XU Ai-qun. Two quite different primary Mn-rich phases in Al-Si-Cu-Mn heat-resistant alloy and its effect to mechanical properties [J]. Materials Science and Engineering A, 2018, 730: 36-40.
- [10] LI Guang-jing, LIAO Heng-cheng, XU Ai-qun, TANG Jing-fan, ZHAO Bao-jun. Peritectic reaction between two primary Mn-rich phases during solidification of Al-Si-Cu-Mn heat-resistant alloy and the effect of cooling rate on it [J]. Journal of Alloys and Compounds, 2018, 753: 239-246.
- [11] LIAO Heng-cheng, HU Yi-yun, HE Zhi-cheng, TANG Yun-yi, LI Guang-jing. Effect of Mn content on microstructure and heat-resistance of near eutectic Al–Si–Mn–Cu alloy [J]. Foundry Technology, 2017, 38(6): 2586–2590. (in Chinese)
- [12] LIAO Heng-cheng, XU He-ting, HU Yi-yun. Effect of RE addition on solidification process and high-temperature strength of Al-12%Si-4%Cu-1.6%Mn heat-resistant alloy [J]. Transactions of Nonferrous Metals Society of China, 2019, 29(6): 1117-1126.
- [13] LIAO Heng-cheng, SUN Guo-xiong. Mutual poisoning effect between Sr and B in Al-Si casting alloys [J]. Scripta Materialia, 2003, 48(8): 1035–1039.
- [14] TAO Shi-wen, PAN Ye, LU Tao, CHEN Yu, WU Ji-li. Microstructures and mechanical properties of La added

- Al-Si casting alloys and mechanism of grain refinement [J]. International Journal of Cast Metals Research, 2015, 28(6): 375-381.
- [15] CHEN Yu, PAN Ye, LU Tao, TAO Shi-wen, WU Ji-li. Effects of combinative addition of lanthanum and boron on grain refinement of Al–Si casting alloys [J]. Materials & Design, 2014, 64: 423–426.
- [16] LI Peng-ting, LI Chong, NIE Jin-feng, JUN Qu-yang, LIU Xiang-fa. Growth and design of LaB₆ microcrystals by aluminum melt reaction method [J]. CrystEngComm, 2013, 15(2): 411–420.
- [17] LI Peng-ting, TIAN Wen-jie, WANG Dong, LIU Xiang-fa. Grain refining potency of LaB₆ on aluminum alloy [J]. Journal of Rare Earths, 2012, 30(11): 1172–1176.
- [18] JING Li-jun, PAN Ye, LU Tao, LI Chen-lin, PI Jing-hong, SHENG Ning-yue. Application of Al-2La-1B grain refiner to Al-10Si-0.3Mg casting alloy [J]. Journal of Materials Engineering and Performance, 2018, 27(6): 2838–2843.
- [19] JING Li-jun, PAN Ye, LU Tao, PI Jing-hong, GU Teng-fei. Nucleation potency prediction of LaB₆ with E2EM model and its influence on microstructure and tensile properties of Al-7Si-0.3Mg alloy [J]. Transactions of Nonferrous Metals Society of China, 2018, 28(9): 1687–1694.
- [20] ZHANG M X, KELLY P M, EASTON M A, TAYLOR J A. Crystallographic study of grain refinement in aluminum alloys using the edge-to-edge matching model [J]. Acta Materialia, 2005, 53(5): 1427–1438.
- [21] ZHANG M X, KELLY P M. Edge-to-edge matching and its applications: Part I. Application to the simple HCP/BCC system [J]. Acta Materialia, 2005, 53(4): 1073–1084.
- [22] ZHANG M X, KELLY P M. Edge-to-edge matching and its applications: Part II. Application to Mg-Al, Mg-Y and Mg-Mn alloys [J]. Acta Materialia, 2005, 53(4): 1085-1096.
- [23] ZHANG M X, KELLY P M, QIAN M, TAYLOR J A. Crystallography of grain refinement in Mg-Al based alloys [J]. Acta Materialia, 2005, 53(11): 3261-3270.
- [24] QIU D, ZHANG M X, TAYLOR J A, KELLY P M. A new approach to designing a grain refiner for Mg casting alloys and its use in Mg-Y-based alloys [J]. Acta Materialia, 2009, 57(10): 3052–3059.
- [25] QIU D, TAYLOR J A, ZHANG M X. Understanding the co-poisoning effect of Zr and Ti on the grain refinement of cast aluminum alloys [J]. Metallurgical and Materials Transactions A, 2010, 41(13): 3412–3421.
- [26] XIAO Zheng-bing, DENG Yun-lai, TANG Jian-guo, CHEN Qi, ZHANG Xin-ming. Poisoning mechanism of Zr on grain refiner of Al-Ti-C and Al-Ti-B [J]. The Chinese Journal of Nonferrous Metals, 2012, 22(2): 371–378. (in Chinese)
- [27] WANG Feng, QIU Dong, LIU Zhi-lin, TARYLOR J A, EASTON M A, ZHANG Ming-xing. The grain refinement mechanism of cast aluminium by zirconium [J]. Acta Materialia, 2013, 61(15): 5636–5645.
- [28] WANG Feng, QIU Dong, LIU Zhi-lin, TARYLOR J, EASTON M, ZHANG Ming-xing. Crystallographic study of Al3Zr and Al3Nb as grain refiners for Al alloys [J]. Transactions of Nonferrous Metals Society of China, 2014, 24(7): 2034–2040.
- [29] ZHU Yu-man, ZHANG Wen-zheng, YE Fei. Study of orientation relationship between β-FeSi₂ thin film and Si

- substrate [J]. Journal of Materials Science and Engineering A, 2003, 21(5): 635-639. (in Chinese)
- [30] LI Guang-jing, LIAO Heng-cheng, SUO Xiao-jing, TANG Yun-yi, DIXIT U S, PETROV P. Cr-induced morphology

change of primary Mn-rich phase in Al-Si-Cu-Mn heat resistant aluminum alloys and its contribution to high temperature strength [J]. Materials Science and Engineering: A, 2018, 709: 90-96.

采用 E2EM 模型预测 LaB₆ 相作为 Al-Si-Cu-Mn 耐热铝合金中初生富 Mn 相形核基底潜力及其细化效果

李广敬,廖恒成

东南大学 材料科学与工程学院 江苏省先进金属材料高技术研究重点实验室,南京 211189

摘 要:通过 E2EM 模型预测 LaB₆ 相作为 Al-Si-Cu-Mn 耐热铝合金在凝固过程中出现的初生 Al₁₃Mn₄Si₈ 相异质 形核基底的潜力。LaB₆ 相和 Al₁₃Mn₄Si₈ 相间共有 5 对位向关系满足 E2EM 模型的判定标准,其中一对晶面关系 ((110)_{LaB₆}//(110)_{Al13Mn₄Si₈)被 TEM 观察证实。这表明 LaB₆ 相可作为 Al₁₃Mn₄Si₈ 相的有效异质形核基底。将 1.0%(质量分数)的 Al-2La-1B 中间合金添加到 Al-12Si-4Cu-2Mn 合金中,并通过组织观察和力学性能测试来评价细化效果。实验结果表明,添加 Al-2La-1B 中间合金能显著细化初生 Al₁₃Mn₄Si₈ 相,证实 E2EM 模型预测的结果。但 初生 Al₁₃Mn₄Si₈ 相的细化并没有提高合金的强度,这是由于铝基体与初生 Al₁₃Mn₄Si₈ 相之间的弹性模量差大于 Al₁₅Mn₃Si₂ 相。}

关键词: E2EM 模型; Al₁₃Mn₄Si₈相; LaB₆相; 耐热铝合金; 显微组织; 力学性能

(Edited by Xiang-qun LI)